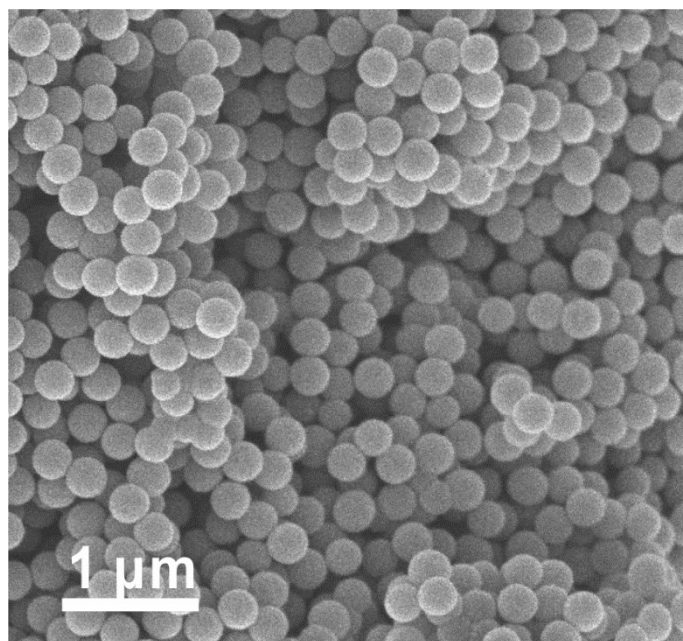# Supporting Information

Table S1. Pt and Ni loading estimated by XRF and elemental analysis of the samples

| Samples	XRF		Elemental analysis		
	Pt /wt%	Ni /wt%	C /wt%	N /wt%	N/C
HPCS	0.0	0.0	88.0	1.5	0.017
$PtNi_0$/HPCS	29.3	0.0			
$PtNi_{0.26}$/HPCS	25.5	1.9			
$PtNi_{0.41}$/HPCS	25.4	3.1			
$PtNi_{1.22}$/HPCS	25.5	9.4	49.2	2.3	0.047
$PtNi_{2.63}$/HPCS	28.2	22.4			
Pt_0Ni/HPCS	0.0	11.1			
$PtNi_{1.22}$/HPCS-no dpa	27.9	10.2	52.6	1.0	0.019
$PtNi_{1.23}$/KB	26.3	9.7			

Figure S1. FESEM image of silica resorcinol-formaldehyde particles $SiO_2@SiO_2/RF$.
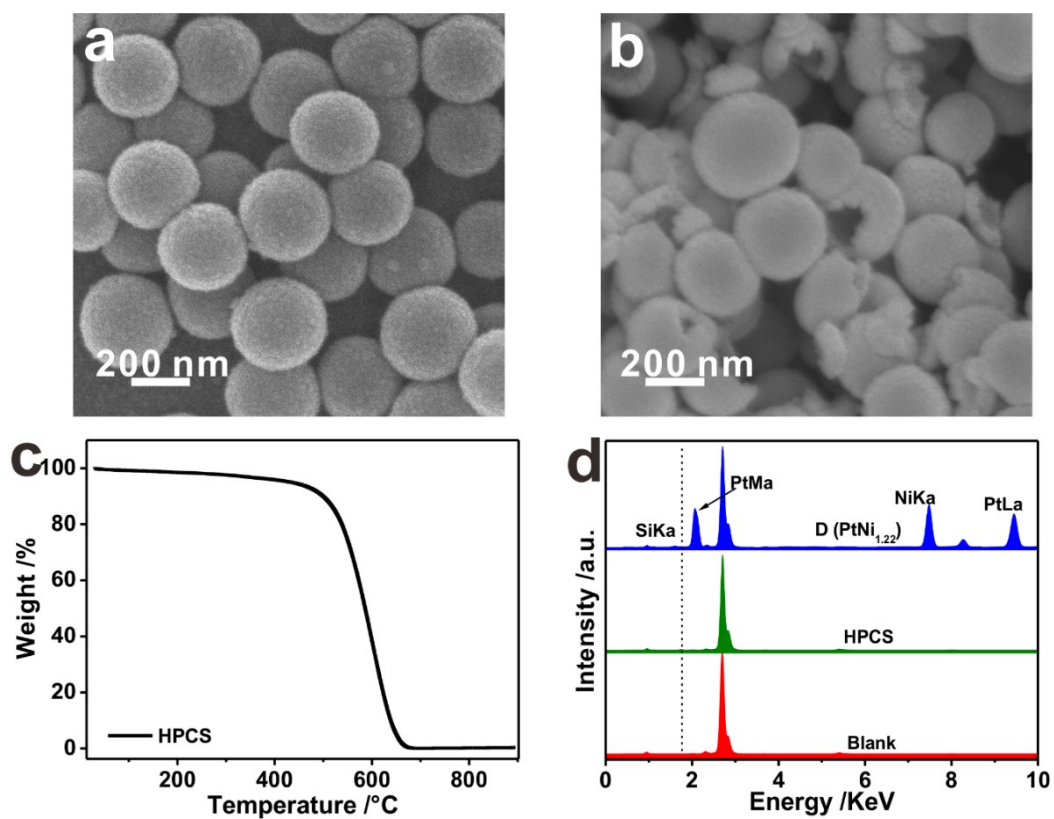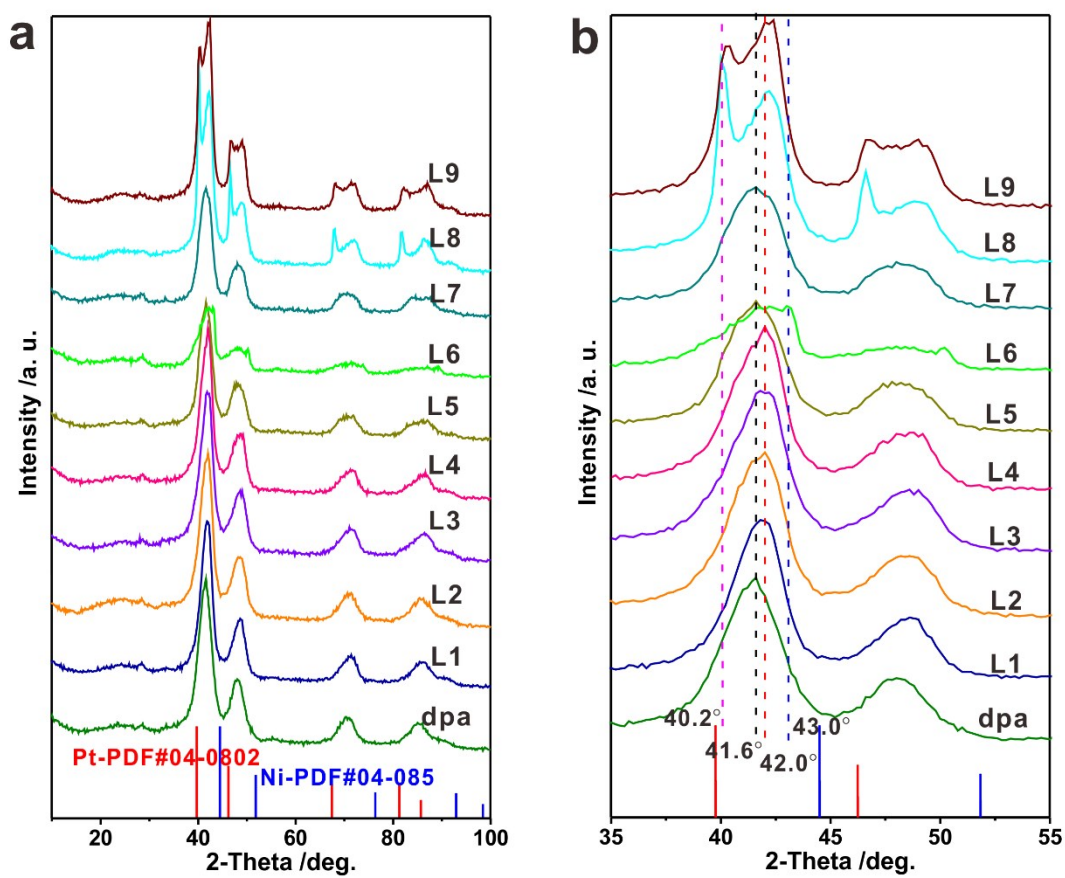

Figure S2. FESEM images of (a) HPCS and (b) HPCS broken by ultrasonication for 4 h after annealing at 973 K for 5 h under Ar. (c) TGA of HPCS in air. (d) XRF of $PtNi_{1.22}/HPCS$ (blue), HPCS (green), and Blank (red).
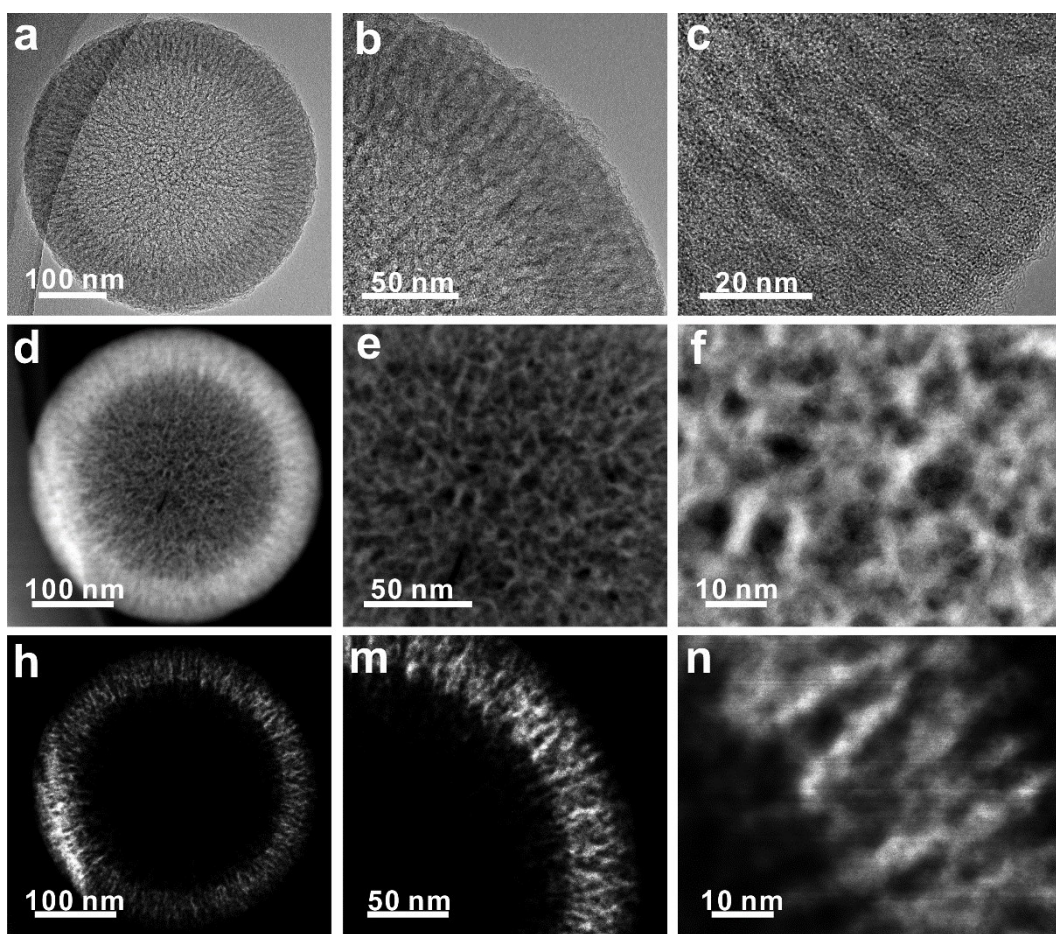
Figure S3. (a–c) TEM images and (d–n) HAADF-STEM images of HPCS.
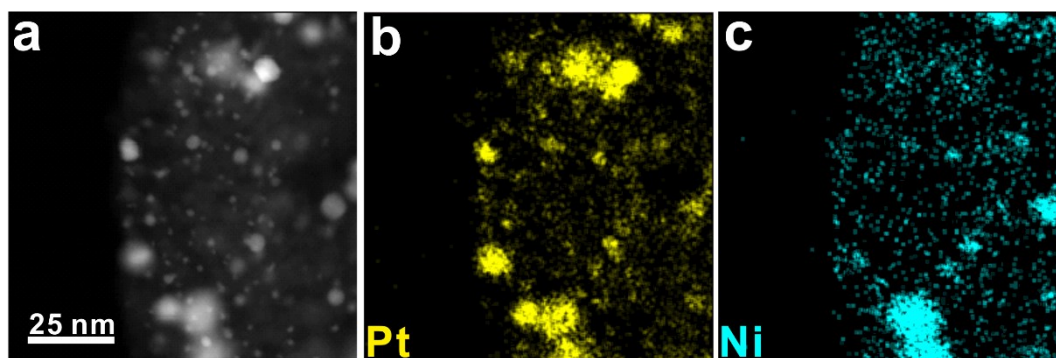
Figure S4. STEM-EDS mapping images of Pt and Ni of PtNi$_{1.22}$/HPCS prepared without dpa (PtNi$_{1.22}$/HPCS-no dpa).
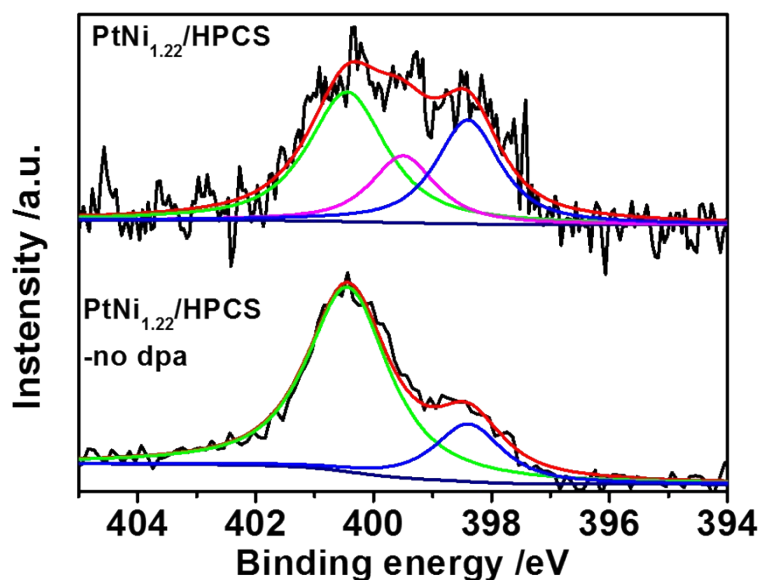
Figure S5. XRD of PtNi$_{1.22}$/HPCS synthesized with different kinds of organic molecules.

dpa: 2,2'-dipyridylamine; L1: aniline; L2: 2-aminopyridine; L3: 2,6-diaminopyridine; L4: pyridine;

L5: diphenylamine; L6: 2,2'-dipicolylamine; L7: benzophenone; L8: benzaldehyde; L9: toluene.
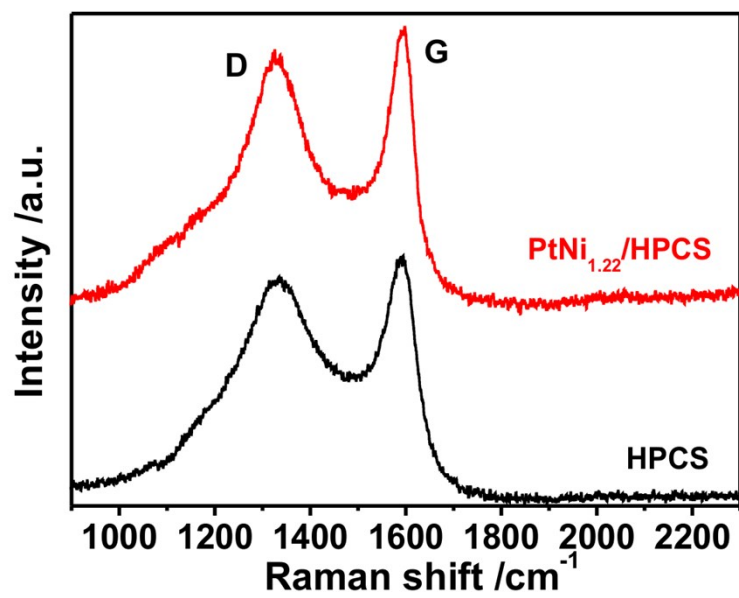
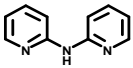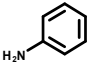**Figure S6.** Raman spectra of HPCS and PtNi$_{1.22}$/HPCS.
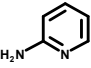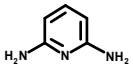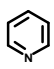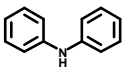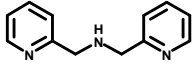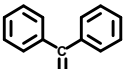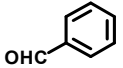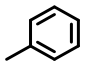
Figure S7. N 1s XPS spectra (black) of PtNi$_{1.22}$/HPCS and PtNi$_{1.22}$/HPCS-no dpa with peak fittings for pyridinic-N (398.4 eV, blue), amino-N (399.5 eV, violet), graphitic-N (400.5 eV, green), background (dark blue) and the fitting spectra (red). The peak positions of all peaks and FWHM of the peak at 399.5 eV (amino-N) were fixed in the fitting process, using an 80% Lorentzian-weighted Gaussian-Lorentzian sum function. A Shirley background was subtracted, and binding energies referenced to C 1s (284.6 eV). FWHM: (PtNi$_{1.22}$/HPCS -no dpa) graphitic-N 1.64 eV, pyridinic-N 1.36 eV; (PtNi$_{1.22}$/HPCS) graphitic-N 1.58 eV, amino-N 1.31 eV (fixed), pyridinic-N 1.3 eV.
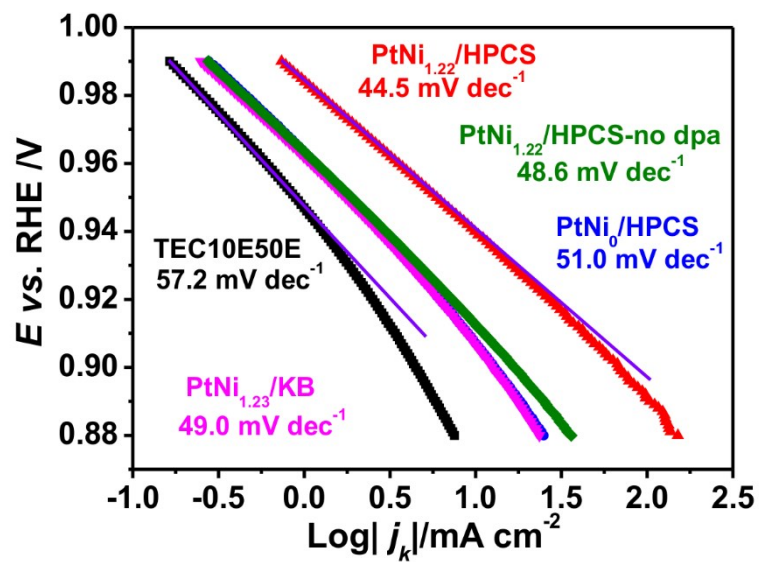
Figure S8. Tafel plots of catalysts PtNi$_0$/HPCS, PtNi$_{1.22}$/HPCS, PtNi$_{1.22}$/HPCS-no dpa, PtNi$_{1.23}$/KB, and TEC10E50E.

Table S2. Comparison of ORR results of prepared catalysts with different kinds of organic molecules

Organic molecules	ECSA /m^2 g^{-1}$_{pt}$	MA /A mg^{-1}$_{Pt}$	SA /mA cm^{-2}$_{Pt}$
2,2'-Dipyridylamine (dpa)	105 ± 8	3.25 ± 0.14	3.11 ± 0.09
Aniline (L1)	81 ± 1	2.55 ± 0.42	2.79 ± 0.42
2-Aminopyridine (L2)	82 ± 1	2.53 ± 0.10	3.10 ± 0.13
2,6-Diaminopyridine (L3)	89 ± 3	3.14 ± 0.14	3.54 ± 0.04
Pyridine (L4)	80 ± 2	2.53 ± 0.27	3.16 ± 0.44
Diphenylamine (L5)	70 ± 1	1.74 ± 0.04	2.48 ± 0.02
2,2'-Dipicolylamine (L6)	30 ± 3	0.66 ± 0.01	2.25 ± 0.16
Benzophenone (L7)	66 ± 1	1.74 ± 0.01	2.62 ± 0.04
Benzaldehyde (L8)	55 ± 1	1.86 ± 0.08	3.42 ± 0.19
Toluene (L9)	62 ± 2	2.01 ± 0.15	3.24 ± 0.12

ECSA, electrochemical surface area; MA, mass activity; SA, specific activity.

Table S3. Comparison of the ORR performance in recently published references.

catalysts	ECSA (m²/g_pt)	MA (mA/μg_Pt)	SA (mA/cm²_Pt)	Reference
Pt₃Fe NW	34.0	2.11	4.34	[1]
PtNi frame	73.4	1.51	2.05	[2]
PtNi frame	54.8	0.24	0.44	[3]
PtNiCo NW	82.2	4.2	5.11	[4]
Rh-Pt NW	86.4	1.41	1.63	[5]
PtNiPd NW	55.4	1.93	3.48	[6]
Pt₃Co NW	52.1	3.71	7.12	[7]
Jagged Pt NW	118	13.6	11.5	[8]
PtPb/Pt plate	55.1	4.3	7.8	[9]
Mo-Pt₃Ni	67.5	6.98	10.3	[10]
Pt Nanocage	38.2	0.75	1.98	[11]
PtNi thin film	9	0.216	2.4	[12]
Pt Nanotube	34.2	0.5	1.48	[13]
PtNi-NiB NP	59	5.3	9.05	[14]
Pt Nanocage	45.2	1.12	2.48	[15]
Pt₇₃Ni₂₇/C-Octahedral	32	1.69	5.29	[16]
PtNi-BNCs	68.2	3.52	5.16	[17]
Pt/NHCS	193 ± 29	0.68 ± 0.14	0.41 ± 0.06	[18]
Pt_seed/Pt₃NiMo/HGS	55	0.7	1.23	[19]
TEC10E50E	65.19 ± 3.64	0.24 ± 0.00	0.37 ± 0.03	This work
PtNi₁.₂₂/HPCS	104.65 ± 7.81	3.25 ± 0.14	3.11 ± 0.09	This work
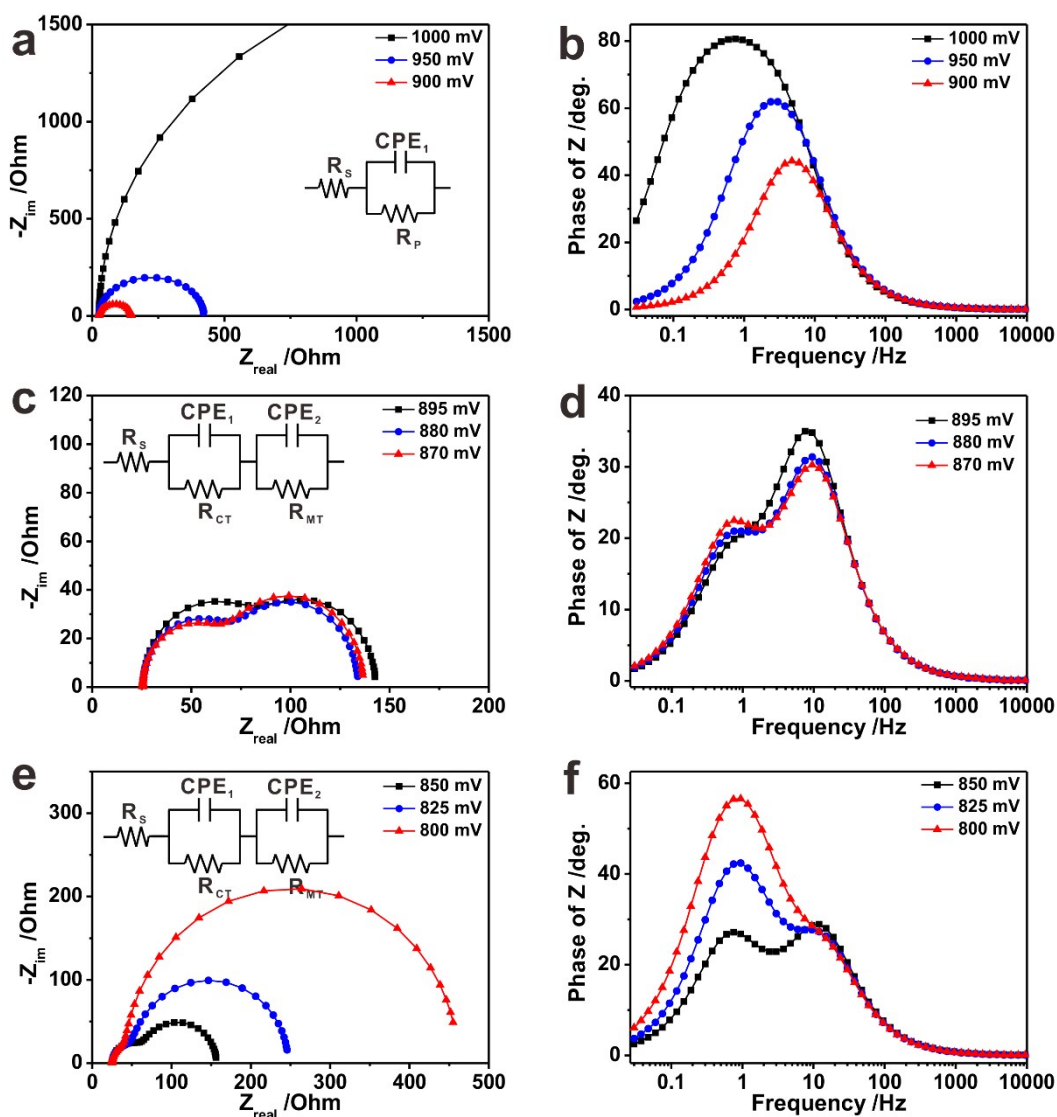
Figure S9. Nyquist plots and Bode phase plots of PtNi$_{1.22}$/HPCS in the (a, b) kinetic region (1000–900 mV), (c, d) mixed-diffusion region (895–870 mV), and (e, f) mass-transport region (850–800 mV). Inset: equivalent electrical circuit used to model the EIS data, considering solution resistance (R$_S$), polarization resistance (R$_P$), two constant phase elements (CPE$_1$ and CPE$_2$), resistance related to mass transfer (R$_{MT}$), and charge transfer resistance related to the ORR (R$_{CT}$). The EIS measurements were performed in O$_2$-saturated 0.1 M HClO$_4$ solution, over a frequency range of 0.03 Hz to 10 kHz, applying a 10 mV perturbation amplitude.
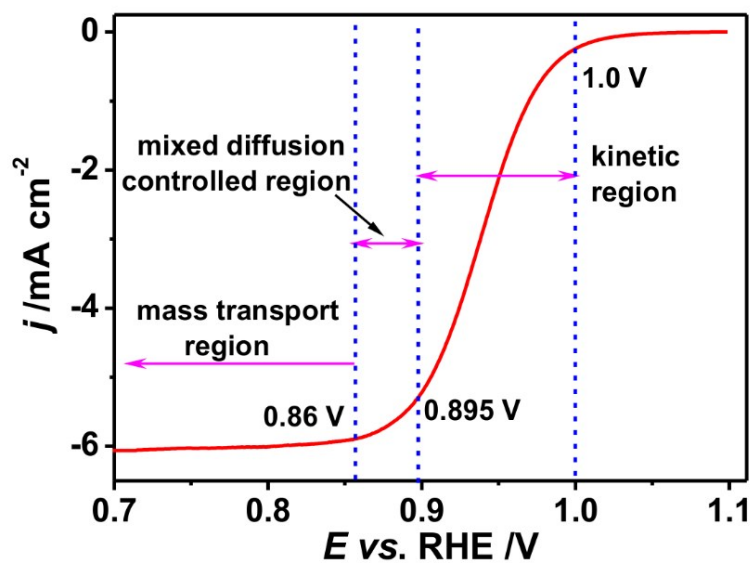
Figure S10. Anodic ORR polarization curves of PtNi$_{1.22}$/HPCS recorded in O$_2$-saturated 0.1 M HClO$_4$ solution with a sweep rate of 10 mV s^{-1} and a rotation rate of 1600 rpm.
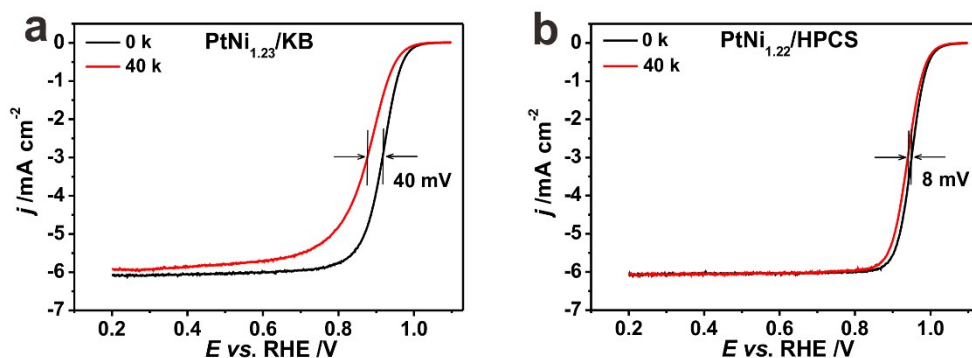
Figure S11. Durability of the catalysts to the ORR. LSV polarization curves of (a) PtNi$_{1.23}$/KB and (b) PtNi$_{1.22}$/HPCS after 0 and 40,000 ADT cycles. LSV recorded in O$_2$-saturated 0.1 M HClO$_4$ solution at a sweep rate of 10 mV s^{-1} and rotation speed of 1600 rpm (293 K). The ADT was conducted at 293 K by applying cyclic sweeps between 0.6 and 1.0 V$_{RHE}$ in O$_2$-saturated 0.1 M HClO$_4$ electrolyte at a sweep rate of 100 mV s^{-1}.
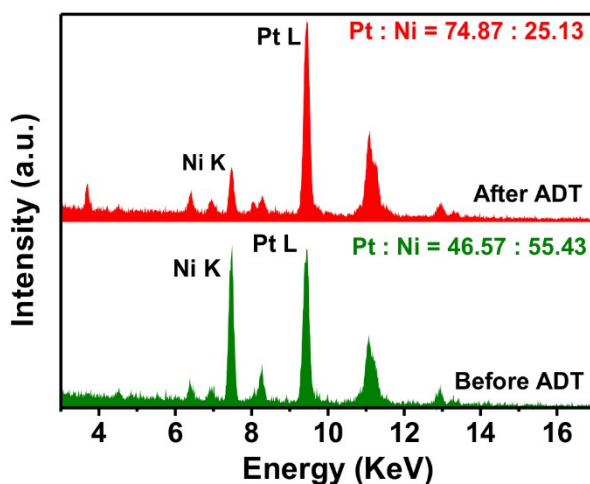
Figure S12. STEM-EDS comparison of PtNi$_{1.22}$/HPCS before (bottom, green) and after (top, red) 60,000 ADT cycles.

Reference:

1. M. Luo, Y. Sun, X. Zhang, Y. Qin, M. Li, Y. Li, C. Li, Y. Yang, L. Wang, P. Gao, G. Lu and S. Guo, *Adv. Mater.*, 2018, **30**, 1705515.
2. H. Kwon, M. K. Kabiraz, J. Park, A. Oh, H. Baik, S.-I. Choi and K. Lee, *Nano Lett.*, 2018, **18**, 2930-2936.
3. S. Chen, Z. Niu, C. Xie, M. Gao, M. Lai, M. Li and P. Yang, *ACS Nano*, 2018, **12**, 8697-8705.
4. K. Jiang, D. Zhao, S. Guo, X. Zhang, X. Zhu, J. Guo, G. Lu and X. Huang, *Sci. Adv.*, 2017, **3**, e1601705.
5. H. Huang, K. Li, Z. Chen, L. Luo, Y. Gu, D. Zhang, C. Ma, R. Si, J. Yang, Z. Peng and J. Zeng, *J. Am. Chem. Soc.*, 2017, **139**, 8152-8159.
6. N. Zhang, Y. Feng, X. Zhu, S. Guo, J. Guo and X. Huang, *Adv. Mater.*, 2017, **29**, 1603774.
7. L. Bu, S. Guo, X. Zhang, X. Shen, D. Su, G. Lu, X. Zhu, J. Yao, J. Guo and X. Huang, *Nat. Commun*, 2016, **7**, 11850.
8. M. Li, Z. Zhao, T. Cheng, A. Fortunelli, C.-Y. Chen, R. Yu, Q. Zhang, L. Gu, B. V. Merinov, Z. Lin, E. Zhu, T. Yu, Q. Jia, J. Guo, L. Zhang, W. A. Goddard, Y. Huang and X. Duan, *Science*, 2016, **354**, 1414-1419.
9. L. Bu, N. Zhang, S. Guo, X. Zhang, J. Li, J. Yao, T. Wu, G. Lu, J.-Y. Ma, D. Su and X. Huang, *Science*, 2016, **354**, 1410-1414.
10. X. Huang, Z. Zhao, L. Cao, Y. Chen, E. Zhu, Z. Lin, M. Li, A. Yan, A. Zettl, Y. M. Wang, X. Duan, T. Mueller and Y. Huang, *Science*, 2015, **348**, 1230-1234.
11. L. Zhang, L. T. Roling, X. Wang, M. Vara, M. Chi, J. Liu, S.-I. Choi, J. Park, J. A. Herron, Z. Xie, M. Mavrikakis and Y. Xia, *Science*, 2015, **349**, 412-416.
12. D. F. van der Vliet, C. Wang, D. Tripkovic, D. Strmcnik, X. F. Zhang, M. K. Debe, R. T. Atanasoski, N. M. Markovic and V. R. Stamenkovic, *Nat. Mater.*, 2012, **11**, 1051-1058.
13. Z. Huang, D. Raciti, S. Yu, L. Zhang, L. Deng, J. He, Y. Liu, N. M. Khashab, C. Wang, J. Gong and Z. Nie, *J. Am. Chem. Soc.*, 2016, **138**, 6332-6335.
14. D. He, L. Zhang, D. He, G. Zhou, Y. Lin, Z. Deng, X. Hong, Y. Wu, C. Chen and Y. Li, *Nat. Commun*, 2016, **7**, 12362.
15. D. S. He, D. He, J. Wang, Y. Lin, P. Yin, X. Hong, Y. Wu and Y. Li, *J. Am. Chem. Soc.*, 2016, **138**, 1494-1497.
16. X. Zhao, S. Takao, K. Higashi, T. Kaneko, G. Samjeskè, O. Sekizawa, T. Sakata, Y. Yoshida, T. Uruga and Y. Iwasawa, *ACS Catal.*, 2017, **7**, 4642-4654.
17. X. Tian, X. Zhao, Y.-Q. Su, L. Wang, H. Wang, D. Dang, B. Chi, H. Liu, E. J. M. Hensen, X. W. Lou and B. Y. Xia, *Science*, 2019, **366**, 850-856.
18. C. Galeano, J. C. Meier, M. Soorholtz, H. Bongard, C. Baldizzone, K. J. J. Mayrhofer and F. Schüth, *ACS Catal.*, 2014, **4**, 3856-3868.
19. J. Knossalla, P. Paciok, D. Göhl, D. Jalalpoor, E. Pizzutilo, A. M. Mingers, M. Heggen, R. E. Dunin-Borkowski, K. J. J. Mayrhofer, F. Schüth and M. Ledendecker, *J. Am. Chem. Soc.*, 2018, **140**, 15684-15689.